Available online at www.sciencedirect.com
SCIENCE DIRECT®
Journal of Sound and Vibration 281 (2005) 849–867
JOURNAL OF SOUND AND VIBRATION
www.elsevier.com/locate/jsvi

Axisymmetric wave propagation in buried, fluid-filled pipes: effects of wall discontinuities

J.M. Muggleton[a,*], M.J. Brennan

[a]*Institute of Sound & Vibration Research, Southampton University, Highfield, Southampton SO17 1BJ, UK*

Received 30 September 2003; accepted 4 February 2004
Available online 12 October 2004

Abstract

Water leakage from buried pipes is a subject of great concern in Britain and across the world because of decreasing water supplies due to changing rainfall patterns, deterioration of antiquated distribution systems, and an increasing population. Correlation techniques are widely used to locate the leaks, however, difficulties are encountered when repairs have been made to a pipe by inserting a new length of pipe to replace a damaged section. Although this practice is now discouraged, the new sections might be of a different material or possibly different cross-section or wall thickness. The wave propagation behaviour at such joints is poorly understood at present.

In earlier work, simple expressions for the wavenumbers of the $s=1$ (fluid-dominated) and $s=2$ (shell dominated) axisymmetric wave types were derived for a fluid-filled elastic pipe, both in vacuo and surrounded by an elastic medium of infinite extent. In this paper, the wave transmission and reflection characteristics of these waves at an axisymmetric pipe wall discontinuity in a fluid-filled piping system are investigated theoretically.

For changes in wall thickness or wall elasticity, simple expressions may be used to characterise the joint. The reason for this is that negligible energy conversion between the wavetypes occurs, so the wavetypes can be considered separately. For changes in the fluid cross-section, significant mode conversion occurs and the wavetypes must be considered together.

*Corresponding author. Tel.: +44-23-8059-2936; fax: +44-23-8059-3190.
E-mail address: jm9@soton.ac.uk (J.M. Muggleton).

0022-460X/$ - see front matter © 2004 Elsevier Ltd. All rights reserved.
doi:10.1016/j.jsv.2004.02.045

1. Introduction

Detection of water leaks in buried pipes is currently a topic of concern in the UK and across the world because of decreasing water supplies due to changing rainfall patterns, deterioration of antiquated distribution systems, and an ever increasing population. Furthermore, leaks are considered to be a public health issue as every puncture in the main is a potential entry point for contaminants.

Detection of water leaks using acoustic methods is now common practice in many countries [1,2]. Correlation techniques are generally used to locate the leaks, and although these techniques have been successful for many years when used with metal pipes, they remain problematic when used with plastic pipes [2,3]. Difficulties are also encountered when repairs have been made to a pipe by inserting a new length of pipe to replace a damaged section. Although this practice is now discouraged, the new sections might be of a different material or possibly different cross-section or wall thickness; the wave propagation behaviour at such joints is poorly understood at present.

A theoretical model of a buried fluid-filled pipe to predict both wavespeed and attenuation has been developed and validated previously by Muggleton et al. [4–6], developing earlier work on an in vacuo pipe by Pinnington and Briscoe [7]. Acoustic energy in buried water pipes generated by a leak propagates at relatively low frequencies, generally less than a few hundred Hz [1–3], and so it is the low-frequency dynamics of the system, well below the ring frequency of the pipe, that is of interest. Well below the pipe ring frequency, four wave types are responsible for the energy transfer [7,8]: three axisymmetric waves, $n=0$, and the $n=1$ wave, related to beam bending. Of the $n=0$ waves, the first, termed $s=1$, is a predominantly fluid borne wave; the second wave, $s=2$, is predominantly a compressional wave in the shell; the third wave, $s=0$, is a torsional wave uncoupled from the fluid. Correlation measurements indicate that leak noise propagates predominantly as the axisymmetric $s=1$ wave, so it is this wave, and its structural counterpart, the $s=2$ wave, which are of most interest in this context. In the earlier work, simple expressions for the wavenumbers of the $s=1$ and $s=2$ axisymmetric wave types were derived for a fluid-filled elastic pipe in vacuo [7], and surrounded by an elastic medium of infinite extent [4].

Textbook solutions are available for the effect of pipe wall discontinuities on the $s=1$ and $s=2$ waves when either the pipe wall can be considered rigid or when the fluid loading on the shell is light; some work has also been undertaken on the effect of pipe wall discontinuities on the propagation of flexural waves in cylindrical shells [9]. In this paper, the wave transmission and reflection characteristics of the $s=1$ and $s=2$ waves at an axisymmetric pipe wall discontinuity are investigated theoretically for a soft-walled pipe, taking into account the coupled nature of the two wavetypes. The discontinuities considered are: a change in wall thickness; a change in pipe wall material elastic modulus; and a change of internal fluid cross-section.

2. Axisymmetric wavenumbers

The pipe equations for $n=0$ axisymmetric wave motion for a fluid filled pipe, both in vacuo and surrounded by an infinite elastic medium have been derived previously [4,7], and expressions for the wavenumbers for the $s=1$ and $s=2$ waves have been found. The derivations are based on simplified forms of Kennard's equations (10) with shell bending neglected, so only valid below the

pipe ring frequency. Furthermore, it is assumed that the frequencies considered are sufficiently low that there is less than one-half of a fluid wavelength across the pipe diameter. For clarity, these results are reproduced in the following subsections. An $e^{i\omega t}$ time dependence is assumed throughout.

2.1. The fluid-borne s=1 wave

For an in vacuo pipe at low frequencies, the $s=1$ wavenumber, k_1, is equal to the free field wavenumber, k_f, modified by a term containing the ratio of the fluid stiffness to the radial pipe wall stiffness:

$$k_1^2 = k_f^2\left(1 + \frac{2B_f/a}{Eh/a^2}\right), \tag{1}$$

where B_f is the bulk modulus of the contained fluid, a and h are the radius and thickness of the shell wall respectively ($h \ll a$), and E is the Young's modulus of the shell material, which may be complex if the material is lossy ($E \to E(1+i\eta)$ where η is the material loss factor). This is the familiar non-dispersive Korteweg equation [11], which can be re-expressed as

$$k_1^2 = k_f^2\left(1 + \frac{z_{\text{fluid}}}{z_{K\text{pipe}}}\right), \tag{2}$$

where the fluid and pipe stiffness impedance terms are given by $z_{\text{fluid}} = -2iB_f/(a\omega)$, $z_{K\text{pipe}} = -iEh/(a^2\omega)$, and ω is the angular frequency. The equation shows that, for a rigid-walled pipe, the $s=1$ wavenumber is equal to the free field wavenumber. As the flexibility of the pipe wall increases, the $s=1$ wavenumber increases, and the wavespeed of the $s=1$ wave decreases correspondingly. The effect of a lossy pipe wall material (represented by a complex Young' modulus) is to introduce a small and negative imaginary component into the wavenumber, indicating that the $s=1$ wave decays as it propagates.

At slightly higher frequencies (but still below the pipe ring frequency), inertial terms must be taken into account, and the wavenumber k_1 becomes

$$k_1^2 = k_f^2\left(1 + \frac{2B_f/a}{Eh/a^2 - \omega^2\rho h}\right) = k_f^2\left(1 + \frac{z_{\text{fluid}}}{z_{\text{pipe}}}\right), \tag{3}$$

where here the pipe impedance term contains a mass element, $z_{M\text{pipe}} = i\rho h\omega$ as well as a stiffness term, so that

$$z_{\text{pipe}} = z_{M\text{pipe}} + z_{K\text{pipe}} = i\left(\rho h\omega - \frac{Eh}{a^2\omega}\right), \tag{4}$$

where ρ is the density of the shell material.

When the pipe is immersed or buried in a surrounding medium, the $s=1$ wavenumber becomes a function of the radiation impedance, z_{rad1}, as well as the fluid and pipe wall impedances:

$$k_1^2 = k_f^2\left(1 + \frac{z_{\text{fluid}}}{z_{\text{pipe}} + z_{\text{rad1}}}\right), \tag{5}$$

where

$$z_{\mathrm{rad1}} = \sum_m \frac{-\mathrm{i}\rho_m c_m k_m}{k^r_{m1}} \frac{H_0(k^r_{m1}a)}{H'_0(k^r_{m1}a)}. \tag{6}$$

ρ_m, c_m, and k_m are the density, wavespeed and wavenumber, respectively of each wavetype present in the surrounding medium, and the summation is performed over all wavetypes present. k^r_{m1}, is the radial component of the wavenumber in the fluid, given by

$$(k^r_{m1})^2 = k^2_m - k^2_1. \tag{7}$$

H_0 is a Hankel function of the second kind, representing outgoing waves when the $\mathrm{e}^{\mathrm{i}\omega t}$ time dependence is adopted, and the prime denotes differentiation with respect to the argument. It is assumed that the surrounding medium is of infinite extent, so that no incoming waves are present.

2.2. The shell-dominated s=2 wave

For an in vacuo pipe, at low frequencies, the $s=2$ wavenumber, k_2, is equal to the 'plate wavenumber', k_L, modified by a term containing the ratio of the fluid stiffness to the radial pipe wall stiffness.

$$k^2_2 = k^2_L\left(1 + \frac{v^2}{1-v^2}\frac{Eh/a^2}{Eh/a^2 + 2B_f/a}\right), \tag{8}$$

where k_L is the wavenumber of a compressional wave in a plate $k^2_L = \omega^2\rho(1-v^2)/E$, and v is the Poisson's ratio of the pipe wall material.

As for the $s=1$ wavenumber, this can be re-expressed in terms of the component impedances defined previously:

$$k^2_2 = k^2_L\left(1 + \frac{v^2}{1-v^2}\frac{z_{K\mathrm{pipe}}}{z_{K\mathrm{pipe}} + z_{\mathrm{fluid}}}\right). \tag{9}$$

Again, at slightly higher frequencies (but still well below the ring frequency), an inertial term must be introduced, giving

$$k^2_2 = k^2_L\left(1 + \frac{v^2}{1-v^2}\frac{z_{K\mathrm{pipe}}}{z_{\mathrm{pipe}} + z_{\mathrm{fluid}}}\right), \tag{10}$$

where $z_{K\mathrm{pipe}}$ has now been replaced by z_{pipe} as defined in Eq. (4).

When the pipe is immersed or buried in a surrounding medium, the $s=2$ wavenumber becomes a function of the radiation impedance, z_{rad2}, as well as the fluid and pipe wall impedances:

$$k^2_2 = k^2_L\left(1 + \frac{v^2}{1-v^2}\frac{z_{K\mathrm{pipe}}}{z_{\mathrm{pipe}} + z_{\mathrm{fluid}} + z_{\mathrm{rad2}}}\right), \tag{11}$$

where

$$z_{\mathrm{rad2}} = \sum_m -\mathrm{i}\rho_m c_m \frac{H_0(k_m a)}{H'_0(k_m a)} \tag{12}$$

The above solutions for the $s=2$ wave are obtained by assuming that the wavenumber k_2 is always smaller than the free-field wavenumbers in the contained fluid and surrounding medium, k_f and k_m, so that $k_2 \ll k_f$ and $k_2 \ll k_m$. For a soft-walled pipe, this may not be true. However, notwithstanding this, the wavenumber estimate will not be substantially in error. The slowest that a compressional wave can travel in a solid is as a longitudinal wave in a rod, $c_L = \sqrt{E/\rho}$, where lateral motion is not constrained; the fastest is as a longitudinal wave in an infinite elastic solid, $c_{\mathrm{BULK}} = \sqrt{E(1-\nu)/(\rho(1+\nu)(1-2\nu))}$, where lateral motion in both directions is constrained. The $s=2$ wavenumber is therefore bounded by

$$\omega\sqrt{\frac{\rho}{E}\frac{(1+\nu)(1-2\nu)}{(1-\nu)}} < k_2 < \omega\sqrt{\frac{\rho}{E}} \tag{13}$$

which for typical values of Poisson's ratio does not present a substantial variation.

3. Wave transmission and reflection at pipe wall discontinuities

In this section, the wave behaviour at a join between two pipes of different material and dimensions is examined. The whole system is assumed to be axisymmetric, so that the pipe

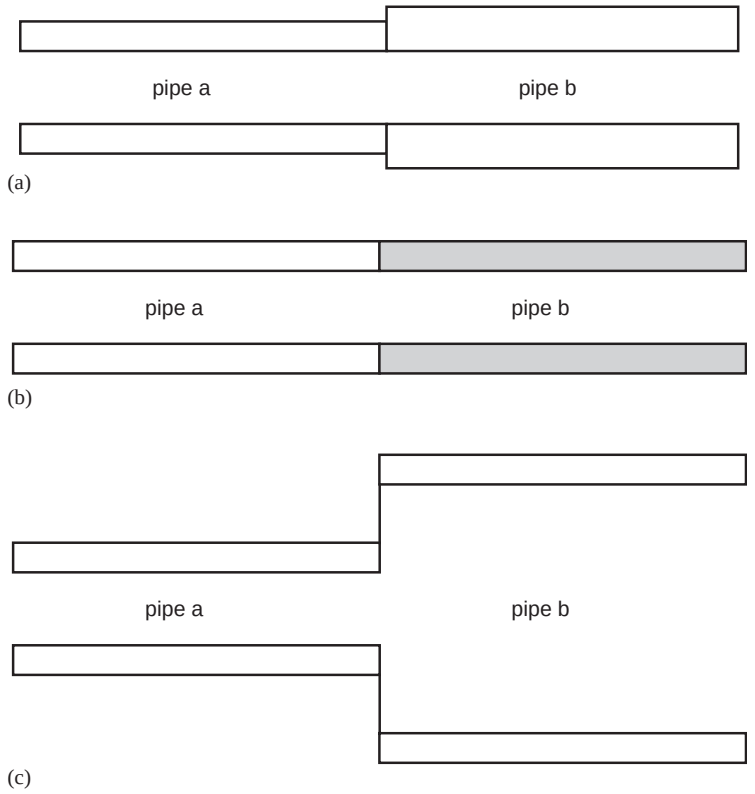

Fig. 1. Axisymmetric pipe discontinuities: (a) wall thickness change; (b) wall elasticity change; (c) internal radius change.

centrelines are continuous at the join, as shown in Fig. 1; furthermore, axisymmetric, $n=0$, incident waves at the discontinuity produce only $n=0$ reflected and transmitted waves. It is assumed that both axisymmetric wavetypes, $s=1$ and $s=2$ may exist in each pipe. Given the coupled nature of the problem, the $s=1$ and $s=2$ waves must be considered together as wave energy may transfer between the two wavetypes (i.e. mode conversion may occur). In this section, a fluid-filled in vacuo pipe is considered. The effects of a surrounding medium are examined in Section 5.

3.1. Pipe state variables for an in vacuo pipe

As well as deriving expressions for the $s=1$ and $s=2$ wavenumbers, Pinnington and Briscoe [7] give expressions for the axial and radial displacements of the pipe wall and the shell axial stress for each wavetype, for an in vacuo pipe. These expressions, together with the expressions for the fluid axial velocity, can be reformulated to give the radial and axial shell velocities and the axial shell force in terms of the wave pressures and the component impedances defined above.

The radial shell velocities for the $s=1$ and $s=2$ waves, W_1 and W_2 respectively, are given by

$$W_1 = P_1 \frac{1}{z_{\text{pipe}}} \quad \text{and} \quad W_2 = -P_2 \frac{1}{z_{\text{fluid}}}, \tag{14a,b}$$

where P_1 and P_2 are the pressure amplitudes of the $s=1$ and $s=2$ waves, respectively. Eq. (14) applies whether the waves are propagating in a positive or negative direction.

The axial shell velocities, U_1 and U_2, are related to the pressures by

$$U_1 = P_1 \frac{-\mathrm{i}\nu}{k_1 a} \frac{1}{z_{\text{pipe}}} \quad \text{and} \quad U_2 = P_2 \frac{\mathrm{i}}{\nu k_2 a} \frac{1}{z_{\text{fluid}}} \left(1 + \frac{(1-\nu^2)(z_{M\text{pipe}} + z_{\text{fluid}})}{z_{K\text{pipe}}}\right). \tag{15a,b}$$

The above equations apply to positive-going waves; for negative-going waves, the sign of the expressions must be reversed.

The axial shell forces, F_1 and F_2, are given by

$$F_1 = P_1 \frac{2\pi\nu}{k_f^2} \frac{z_{M\text{pipe}}}{(z_{\text{fluid}} + z_{\text{pipe}})} \quad \text{and} \quad F_2 = P_2 \frac{2\pi a^2}{\nu} \left(1 + \frac{z_{\text{pipe}}}{z_{\text{fluid}}}\right). \tag{16a,b}$$

As for the radial wall velocities, the above equations apply to both positive- and negative-going waves.

The fluid axial velocities, U_{f1} and U_{f2} are related to the pressures by

$$U_{f1} = P_1 \frac{1}{z_1} \quad \text{and} \quad U_{f2} = P_2 \frac{1}{z_2}, \tag{17a,b}$$

where z_1 and z_2 are the specific acoustic impedances of the $s=1$ and $s=2$ waves respectively, given by

$$z_1 = \sqrt{B_f \rho_f}\, \frac{k_1}{k_f} \quad \text{and} \quad z_2 = \sqrt{B_f \rho_f}\, \frac{k_2}{k_f},$$

ρ_f is the density of the contained fluid.

The above equations apply to positive-going waves; for negative-going waves, the sign of the expressions must be reversed, as for the shell axial velocities.

Any section of pipe, with both positive- and negative-going $s=1$ and $s=2$ waves can now be described by the matrix equation

$$\begin{bmatrix} P \\ F \\ U_f \\ U \end{bmatrix} = \begin{bmatrix} 1 & 1 & 1 & 1 \\ \frac{2\pi v}{k_f^2}\frac{z_{M\text{pipe}}}{(z_{\text{pipe}}+z_{\text{fluid}})} & \frac{2\pi a^2}{v}\left(1+\frac{z_{\text{pipe}}}{z_{\text{fluid}}}\right) & \frac{2\pi v}{k_f^2}\frac{z_{M\text{pipe}}}{(z_{\text{pipe}}+z_{\text{fluid}})} & \frac{2\pi a^2}{v}\left(1+\frac{z_{\text{pipe}}}{z_{\text{fluid}}}\right) \\ \frac{1}{z_1} & \frac{1}{z_2} & -\frac{1}{z_1} & -\frac{1}{z_2} \\ \frac{-iv}{k_1 a}\frac{1}{z_{\text{pipe}}} & \frac{i}{vk_2 a}\frac{1}{z_{\text{fluid}}}\left(1+\frac{(1-v^2)(z_{M\text{pipe}}+z_{\text{fluid}})}{z_{K\text{pipe}}}\right) & \frac{iv}{k_1 a}\frac{1}{z_{\text{pipe}}} & \frac{-i}{vk_2 a}\frac{1}{z_{\text{fluid}}}\left(1+\frac{(1-v^2)(z_{M\text{pipe}}+z_{\text{fluid}})}{z_{K\text{pipe}}}\right) \end{bmatrix} \begin{bmatrix} p_1^+ \\ p_2^+ \\ p_1^+ \\ p_2^+ \end{bmatrix}, \quad (18)$$

where $\begin{bmatrix} P_1^+ \\ P_2^+ \\ P_1^- \\ P_2^- \end{bmatrix}$ is the vector of positive- (superscript $^+$) and negative-going (superscript $^-$) $s=1$ and $s=2$ pressure wave amplitudes, and $\begin{bmatrix} P \\ F \\ U_f \\ U \end{bmatrix}$ is the vector of total pressure, shell axial force, fluid axial velocity and shell axial velocity at any point in the pipe as a result of those waves.

3.2. Changes in pipe wall material or thickness

Consider the junction between two sections of pipe with differing wall material or shell thickness, but with no change in internal cross-section. Continuity and equilibrium considerations indicate that the state vectors $\begin{bmatrix} P \\ F \\ U_f \\ U \end{bmatrix}$ for each pipe section at the join must be equal. Eq. (18) for each pipe section can be re-expressed as

$$\begin{bmatrix} \mathbf{f} \\ \mathbf{u} \end{bmatrix} = \begin{bmatrix} \mathbf{A}_{\text{pipe}} & \mathbf{A}_{\text{pipe}} \\ \mathbf{B}_{\text{pipe}} & -\mathbf{B}_{\text{pipe}} \end{bmatrix} \begin{bmatrix} \mathbf{p}^+ \\ \mathbf{p}^- \end{bmatrix}, \quad (19)$$

where

$$\mathbf{f} = \begin{Bmatrix} P \\ F \end{Bmatrix}, \quad \mathbf{u} = \begin{Bmatrix} U_f \\ U \end{Bmatrix}, \quad \mathbf{p}^+ = \begin{Bmatrix} P_1^+ \\ P_2^+ \end{Bmatrix} \quad \text{and} \quad \mathbf{p}^- = \begin{Bmatrix} P_1^- \\ P_2^- \end{Bmatrix},$$

$$\mathbf{A}_{\text{pipe}} = \begin{bmatrix} 1 & 1 \\ \dfrac{2\pi v}{k_f^2} \dfrac{z_{M\text{pipe}}}{(z_{\text{pipe}} + z_{\text{fluid}})} & \dfrac{2\pi a^2}{v}\left(1 + \dfrac{z_{\text{pipe}}}{z_{\text{fluid}}}\right) \end{bmatrix}$$

and

$$\mathbf{B}_{\text{pipe}} = \begin{bmatrix} \dfrac{1}{z_1} & \dfrac{1}{z_2} \\ \dfrac{-\mathrm{i}v}{k_1 a} \dfrac{1}{z_{\text{pipe}}} & \dfrac{\mathrm{i}}{vk_2 a} \dfrac{1}{z_{\text{fluid}}}\left(1 + \dfrac{(1-v^2)(z_{M\text{pipe}} + z_{\text{fluid}})}{z_{K\text{pipe}}}\right) \end{bmatrix}.$$

Equating the state vectors for each pipe, $\begin{bmatrix} \mathbf{f} \\ \mathbf{u} \end{bmatrix}$, gives

$$\begin{bmatrix} \mathbf{A}_a & \mathbf{A}_a \\ \mathbf{B}_a & -\mathbf{B}_a \end{bmatrix} \begin{bmatrix} \mathbf{p}_a^+ \\ \mathbf{p}_a^- \end{bmatrix} = \begin{bmatrix} \mathbf{A}_b & \mathbf{A}_b \\ \mathbf{B}_b & -\mathbf{B}_b \end{bmatrix} \begin{bmatrix} \mathbf{p}_b^+ \\ \mathbf{p}_b^- \end{bmatrix}, \tag{20}$$

where the subscripts a and b refer to the different sections of pipe shown in Fig. 1. Eq. (20) can be rearranged to give the scattering matrix, **S,** of pressure reflection and transmission coefficients:

$$\begin{bmatrix} \mathbf{P}_a^- \\ \mathbf{P}_b^+ \end{bmatrix} = \mathbf{S} \begin{bmatrix} \mathbf{P}_a^+ \\ \mathbf{P}_b^- \end{bmatrix}, \tag{21}$$

where

$$\mathbf{S} = \begin{bmatrix} \mathbf{r}_{aa} & \mathbf{t}_{ba} \\ \mathbf{t}_{ab} & \mathbf{r}_{bb} \end{bmatrix} = \begin{bmatrix} \mathbf{A}_a & -\mathbf{A}_b \\ -\mathbf{B}_a & -\mathbf{B}_b \end{bmatrix}^{-1} \begin{bmatrix} -\mathbf{A}_a & \mathbf{A}_b \\ -\mathbf{B}_a & -\mathbf{B}_b \end{bmatrix}.$$

Here, $\mathbf{r}_{aa}$ is the reflection coefficient matrix for waves impinging on the joint from pipe a, and being reflected back into pipe a, $\mathbf{r}_{bb}$ is the reflection coefficient matrix for waves impinging on the joint from pipe b, and being reflected back into pipe b, $\mathbf{t}_{ab}$ is the transmission coefficient matrix for waves impinging on the joint from pipe a, and being transmitted to pipe b, and $\mathbf{t}_{ba}$ is the transmission coefficient matrix for waves impinging on the joint from pipe b, and being transmitted to pipe a. Each matrix comprises four elements, relating to the reflection and transmission of $s=1$ or $s=2$ waves. For example,

$$\mathbf{r}_{aa} = \begin{bmatrix} r_{aa11} & r_{aa21} \\ r_{aa12} & r_{aa22} \end{bmatrix}. \tag{22}$$

Here, r_{aa11} is the reflection coefficient for $s=1$ waves being reflected as $s=1$ waves, r_{aa21} is the reflection coefficient for $s=2$ waves being reflected as $s=1$ waves, r_{aa12} is the reflection coefficient for $s=1$ waves being reflected as $s=2$ waves, and r_{aa22} is the reflection coefficient for $s=2$ waves being reflected as $s=2$ waves.

Provided the matrix $\begin{bmatrix} \mathbf{A}_a & -\mathbf{A}_b \\ -\mathbf{B}_a & -\mathbf{B}_b \end{bmatrix}$ in Eq. (21) is non-singular, the scattering matrix can be solved numerically.

3.3. Changes in internal cross-section

When the pipe discontinuity comprises a change in internal cross-section, the state vector described in the previous subsection is no longer equal either side of the join. Here, a slightly modified form must be used. Continuity of fluid pressure and shell axial velocity still apply, but the shell force is no longer continuous, nor is the fluid axial velocity.

In place of the shell force, the total axial force on the fluid/shell system must be used; equilibrium states that this must be continuous across the discontinuity. The total axial force, F_{tot}, is given in terms of the shell axial force, F, and the fluid pressure, P, as

$$F_{\text{tot}} = F - \pi a^2 P. \tag{23}$$

In place of fluid axial velocity, the fluid volume velocity relative to the shell wall remains continuous across the discontinuity. This relative volume velocity, Q_{rel}, is given in terms of the fluid and shell axial velocities, U_f and U respectively as

$$Q_{\text{rel}} = (U_f - U)\pi a^2. \tag{24}$$

Following the same procedure as in the previous subsection, the scattering matrix is now given by

$$\mathbf{S} = \begin{bmatrix} \mathbf{C}_a & -\mathbf{C}_b \\ -\mathbf{D}_a & -\mathbf{D}_b \end{bmatrix}^{-1} \begin{bmatrix} -\mathbf{C}_a & \mathbf{C}_b \\ -\mathbf{D}_a & -\mathbf{D}_b \end{bmatrix}, \tag{25}$$

where

$$\mathbf{C}_{\text{pipe}} = \begin{bmatrix} 1 & 1 \\ \dfrac{2\pi v}{k_f^2} \dfrac{z_{M\text{pipe}}}{(z_{\text{pipe}} + z_{\text{fluid}})} - \pi a^2 & \dfrac{2\pi a^2}{v}\left(1 + \dfrac{z_{\text{pipe}}}{z_{\text{fluid}}}\right) - \pi a^2 \end{bmatrix}$$

and

$$\mathbf{D}_{\text{pipe}} = \begin{bmatrix} \pi a^2\left(\dfrac{1}{z_1} + \dfrac{\mathrm{i}v}{k_1 a}\dfrac{1}{z_{\text{pipe}}}\right) & \pi a^2\left(\dfrac{1}{z_2} - \dfrac{\mathrm{i}}{vk_2 a}\dfrac{1}{z_{\text{fluid}}}\left(1 + \dfrac{(1-v^2)(z_{M\text{pipe}} + z_{\text{fluid}})}{z_{K\text{pipe}}}\right)\right) \\ \dfrac{-\mathrm{i}v}{k_1 a}\dfrac{1}{z_{\text{pipe}}} & \dfrac{\mathrm{i}}{vk_2 a}\dfrac{1}{z_{\text{fluid}}}\left(1 + \dfrac{(1-v^2)(z_{M\text{pipe}} + z_{\text{fluid}})}{z_{K\text{pipe}}}\right) \end{bmatrix}$$

and the $\mathbf{C}$ and $\mathbf{D}$ are evaluated separately for each pipe section. Again, this can be solved numerically provided $\begin{bmatrix} \mathbf{C}_a & -\mathbf{C}_b \\ -\mathbf{D}_a & -\mathbf{D}_b \end{bmatrix}$ is non-singular. The scattering matrix as given by Eq. (25) is the more general form of the scattering matrix, valid for changes in wall thickness and wall elasticity as well as changes in internal cross-section.

3.4. Power reflection and transmission coefficients

Given the coupled nature of the problem, the join reflection and transmission characteristics can be more usefully described in terms of reflection and transmission of vibrational power rather than pressure amplitudes.

For the $s=1$ wave, although vibration of both the fluid and shell occur, the energy is predominantly in the fluid [7]; the average energy flow per unit time, ε_1, is therefore given in terms of the $s=1$ pressure amplitude, P_1, by

$$\varepsilon_1 \approx \tfrac{1}{2}\mathrm{Re}\{P_1^* U_1\}\pi a^2 = \tfrac{1}{2}|P_1|^2 \frac{\pi a^2}{\rho_f \omega}\,\mathrm{Re}\{k_1\} = \tau_1 |P_1|^2. \tag{26}$$

Likewise, for the $s=2$ wave, vibration of both the fluid and the shell occur; for this wave, however, the energy is predominantly associated with the axial shell motion; the average energy flow per unit time, ε_2, is therefore given in terms of the $s=2$ axial shell velocity U_2 by

$$\varepsilon_2 \approx \tfrac{1}{2}\mathrm{Re}\{F_2 U_2^*\} = \tfrac{1}{2}|U_2|^2 2\pi a h \rho\omega \mathrm{Re}\left\{\frac{1}{k_2}\right\} \tag{27}$$

or, in terms of the pressure amplitude, from Eq. (15)

$$\varepsilon_2 \approx \tfrac{1}{2}|P_2|^2 2\pi a h \rho\omega \left|\frac{1}{(\nu k_2 a z_{\mathrm{fluid}})}\left(1+\frac{(1-\nu^2)(z_{M\mathrm{pipe}}+z_{\mathrm{fluid}})}{z_{K\mathrm{pipe}}}\right)\right|^2 \mathrm{Re}\left\{\frac{1}{k_2}\right\} = \tau_2 |P_2|^2. \tag{28}$$

The pressure reflection and transmission coefficients, $\mathbf{r}$ and $\mathbf{t}$, can now be related to power reflection and transmission coefficients, $\mathbf{R}$ and $\mathbf{T}$, at the discontinuity:

$$\begin{bmatrix} \mathbf{R}_{aa} & \mathbf{T}_{ba} \\ \mathbf{T}_{ab} & \mathbf{R}_{bb} \end{bmatrix} = \begin{bmatrix} R_{aa11} & R_{aa21} & T_{ba11} & T_{ba21} \\ R_{aa12} & R_{aa11} & T_{ba12} & T_{ba22} \\ T_{ab11} & T_{ab21} & R_{bb11} & R_{bb21} \\ T_{ab12} & T_{ab22} & R_{bb12} & R_{bb22} \end{bmatrix}$$

$$= \begin{bmatrix} |r_{aa11}|^2 & \frac{\tau_{1a}}{\tau_{2a}}|r_{aa21}|^2 & \frac{\tau_{1a}}{\tau_{1b}}|t_{ba11}|^2 & \frac{\tau_{1a}}{\tau_{2b}}|t_{ba21}|^2 \\ \frac{\tau_{2a}}{\tau_{1a}}|r_{aa12}|^2 & |r_{aa22}|^2 & \frac{\tau_{2a}}{\tau_{1b}}|t_{ba12}|^2 & \frac{\tau_{2a}}{\tau_{2b}}|t_{ba22}|^2 \\ \frac{\tau_{1b}}{\tau_{1a}}|t_{ab11}|^2 & \frac{\tau_{1b}}{\tau_{2a}}|t_{ab21}|^2 & |r_{bb11}|^2 & \frac{\tau_{1b}}{\tau_{2b}}|r_{bb21}|^2 \\ \frac{\tau_{2b}}{\tau_{1a}}|t_{ab12}|^2 & \frac{\tau_{2b}}{\tau_{2a}}|t_{ab22}|^2 & \frac{\tau_{2b}}{\tau_{1b}}|r_{bb12}|^2 & |r_{bb22}|^2 \end{bmatrix}, \tag{29}$$

where, as before, the a and b subscripts relate to the different sections of pipe.

4. Simulations

Example results are presented here for a number of pipe configurations. In each case the pipes are considered to be of semi-infinite extent on either side of the discontinuity.

The first consists of a water-filled MDPE pipe coupled to a steel pipe of the same dimensions, in vacuo. The material and geometrical properties of the pipes are shown in Tables 1a and 1b.

Figs. 2a and b show the real parts of the predicted wavenumbers of the $s=1$ and $s=2$ waves respectively as a function of the non-dimensionalised fluid wavenumber, $k_f a$, for both the MDPE and steel pipes. The figures show that, as expected, the $s=1$ wavenumber for the steel pipe is very close to the fluid wavenumber; the $s=1$ wavenumber for the MDPE pipe is substantially larger due to the greater flexibility of the pipe walls. The $s=1$ wavenumber for the MDPE pipe is slightly dispersive, as the wavenumber curve deviates slightly from a straight line. The $s=2$ wavenumbers, as expected, are almost identical to the respective plate wavenumbers with the difference for the MDPE pipe being undetectable on the figure. Neither wavenumbers exhibit perceptible dispersive behaviour.

Figs. 3a–d show the power reflection and transmissions coefficients for the pipe coupling as a function of the non-dimensionalised fluid wavenumber. The figures show that, for waves

Table 1
Geometrical and material properties

(a) *Of the MDPE pipe*	
Wall thickness/radius	0.1
Density (kg/m^3)	900
Young's Modulus (GN/m^2)	1.6
Poisson's ratio	0.4
(b) *Of the steel pipe*	
Wall thickness/radius	0.1
Density (kg/m^3)	7800
Young's Modulus (GN/m^2)	207
Poisson's ratio	0.3

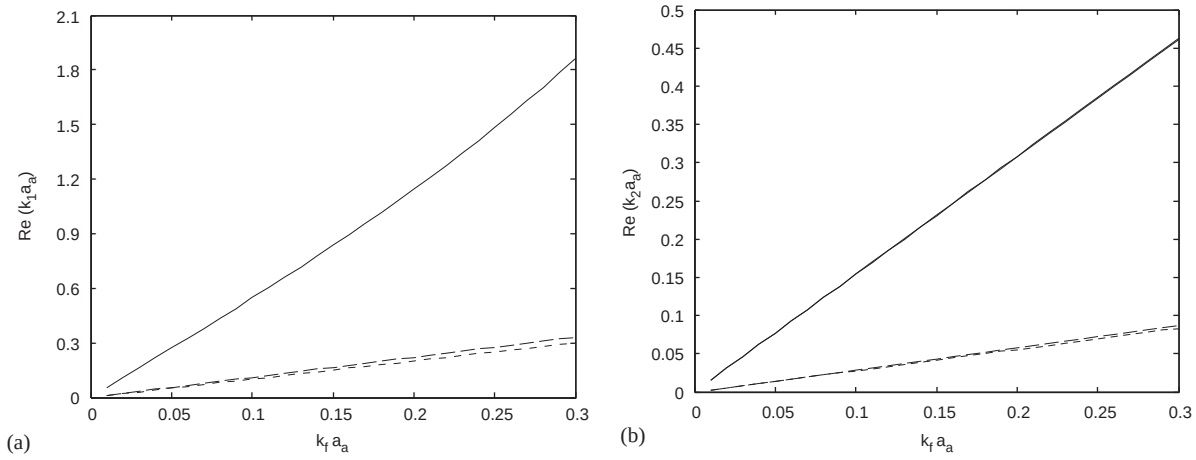

Fig. 2. (a) Real part of $s=1$ wavenumbers for MDPE and steel pipes. ——, MDPE pipe; – – –, steel pipe; - - - - -, fluid wavenumber. (b) Real part of $s=2$ wavenumbers for MDPE and steel pipes. ——, MDPE pipe and MDPE pipe plate wave (indistinguishable in the wavenumber range depicted); – – –, steel pipe; - - - - -, steel pipe plate wave.

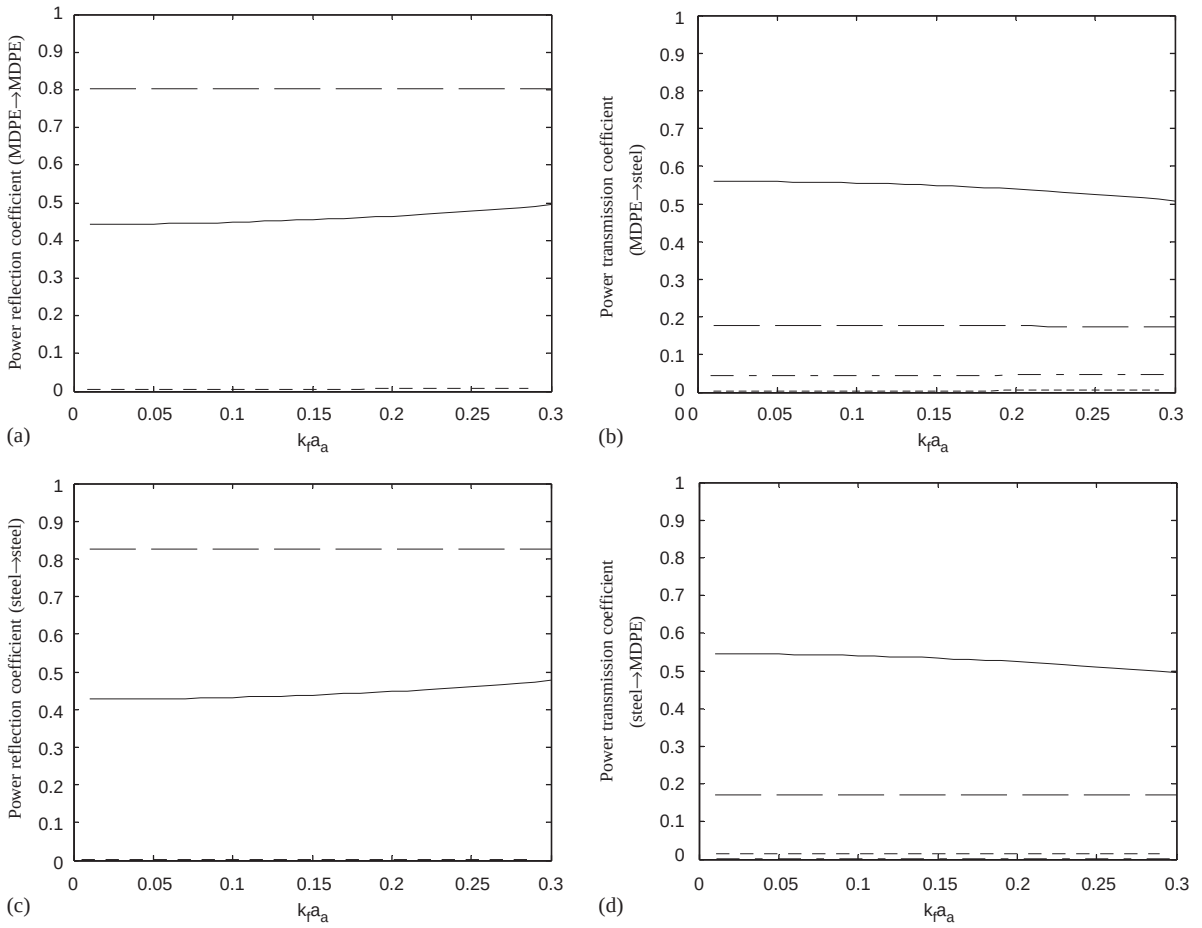

Fig. 3. (a) Power reflection coefficients for MDPE/steel pipe (MDPE pipe → MDPE pipe). ——, $s_1 \rightarrow s_1$; – – –, $s_2 \rightarrow s_2$; - - - - -, $s_1 \rightarrow s_2$; - - - - -, $s_2 \rightarrow s_1$. (b) Power transmission coefficients for MDPE/steel pipe (MDPE pipe → steel pipe). ——, $s_1 \rightarrow s_1$; – – –, $s_2 \rightarrow s_2$; - - - - -, $s_1 \rightarrow s_2$; – - – - –, $s_2 \rightarrow s_1$. (c) Power reflection coefficients for MDPE/steel pipe (steel pipe → steel pipe). ——, $s_1 \rightarrow s_1$; – – –, $s_2 \rightarrow s_2$; - - - - -, $s_1 \rightarrow s_2$; - - - - -, $s_2 \rightarrow s_1$. (d) Power transmission coefficients for MDPE/steel pipe (steel pipe → MDPE pipe). ——, $s_1 \rightarrow s_1$; – – –, $s_2 \rightarrow s_2$; - - - - -, $s_1 \rightarrow s_2$; – - – - –, $s_2 \rightarrow s_1$.

travelling in both directions, the s_2–s_2 power reflection coefficients ($s = 2$ waves being reflected as $s = 2$ waves) is large (~0.8 in both cases); this is to be expected, given the large change in pipe wall stiffness. The s_1–s_1 reflection coefficients in each direction are slightly smaller (~0.4 to 0.5), resulting from the abrupt change in wavenumber at the discontinuity. The cross-terms (s_1–s_2 and vice versa) are small, indicating that there is very little mode conversion, so simple transmission and reflection of each wavetype independently occurs at the discontinuity. The reflection and transmission coefficients vary very little with frequency, the changes that are observed corresponding with the nonlinear variation of wavenumber with frequency observed in Figs. 2a and b. In the case of the transmission coefficients, the values obtained are independent of the direction of wave propagation, as would be expected.

Given the small variations of reflection and transmission coefficients with frequency, the subsequent investigations in this section are carried out at a single frequency.

4.1. Variation with pipe wall thickness

In this section, the effects of changes in wall thickness are examined. Figs. 4a and b show the power reflection and transmissions coefficients for the MDPE pipe described in Table 1a coupled to a similar pipe with a different wall thickness. The results are shown as a function of wall thickness ratio, for $k_f a_a = 0.2$. As expected, the s_1–s_1 and s_2–s_2 reflection coefficients increase with increasing change in wall thickness. The transmission coefficients decrease correspondingly. The cross-terms were found to be negligible and hence are not shown in the figures. This is as expected, given that there is no mechanism for mode conversion at the discontinuity as the boundary conditions for the shell and the fluid are independent. For the fluid, the predominant reason that reflection occurs is because the $s = 1$ wavenumber changes. The power reflection and transmission coefficients for a simple wavenumber change (as might be encountered at a boundary between two different media) are given by

$$R_{aa11} = \left(\frac{1 - k_{b1}/k_{a1}}{1 + k_{b1}/k_{a1}}\right)^2 \quad \text{and} \quad T_{ab11} = \frac{4k_{b1}/k_{a1}}{(1 + k_{b1}/k_{a1})^2}. \tag{30a,b}$$

For the shell, the wavenumber does not change significantly (the plate wavenumber, k_L, being independent of the shell thickness), but the shell thickness changes. The power reflection and transmission coefficients for a simple thickness change are given by

$$R_{aa22} = \left(\frac{1 - h_b/h_a}{1 + h_b/h_a}\right)^2 \quad \text{and} \quad T_{ab22} = \frac{4h_b/h_a}{(1 + h_b/h_a)^2}. \tag{31a,b}$$

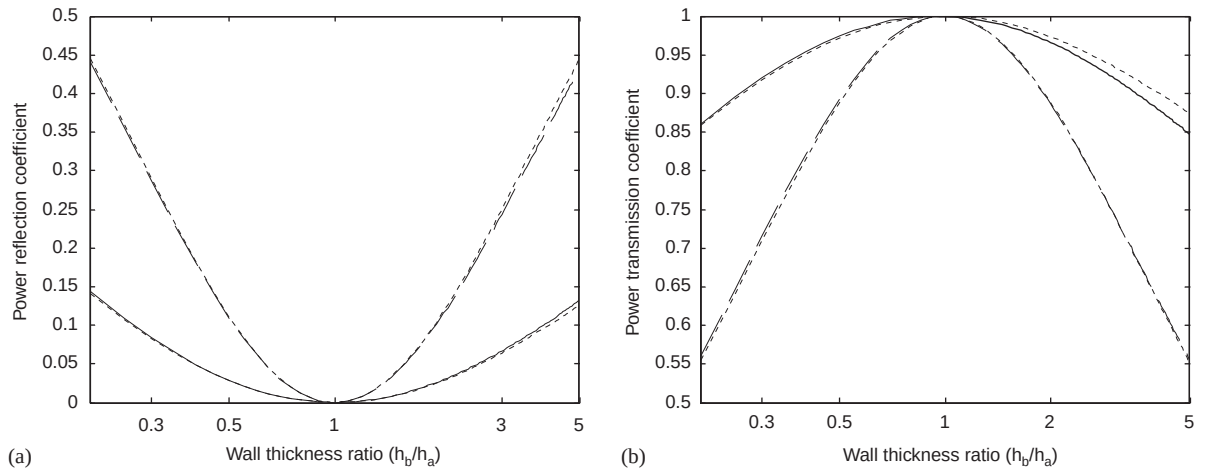

Fig. 4. (a) Power reflection coefficients for MDPE pipe. ——, $s_1 \rightarrow s_1$; – – –, $s_2 \rightarrow s_2$; - - - - -, uncoupled approximations. (b) Power transmission coefficients for MDPE pipe. ——, $s_1 \rightarrow s_1$; – – –, $s_2 \rightarrow s_2$; - - - - -, uncoupled approximations.

The above reflection and transmission coefficients are also plotted in the figures, confirming the mechanisms for reflection and transmission.

4.2. Variation with pipe wall elastic modulus

Here, the effects of changes in wall elastic modulus are examined. Figs. 5a and b show the power reflection and transmissions coefficients for the MDPE pipe described in Table 1a coupled to a similar pipe with a different elastic modulus. The results are shown as a function of wall stiffness ratio, for $k_f a_a = 0.2$. As expected, the s_1–s_1 and s_2–s_2 reflection coefficients increase with increasing change in elastic modulus. The transmission coefficients decrease correspondingly. Again the cross-terms are negligible, indicating very little mode conversion at the discontinuity, and not shown on the figures. As for changes in wall thickness, this is as expected, given that the boundary conditions for the shell and the fluid are independent. As before, for the fluid, the predominant reason that reflection occurs is because the $s = 1$ wavenumber changes. For the shell also, only the wavenumber changes.

The power reflection and transmission coefficients for the wavenumber changes only (Eqs. (30a,b)) are also shown in the figures, confirming the mechanisms for reflection and transmission. If the shell was completely unloaded by the fluid, the power reflection and transmission coefficients could be expressed in terms of the pipe wall elastic moduli as

$$R_{aa22} = \left(\frac{1-\sqrt{E_b/E_a}}{1+\sqrt{E_b/E_a}}\right)^2 \quad \text{and} \quad T_{ab22} = \frac{4\sqrt{E_b/E_a}}{(1+\sqrt{E_b/E_a})^2}. \tag{32a,b}$$

These are also plotted, confirming that the effect of the fluid loading on the reflection and transmission coefficients is shell is very small.

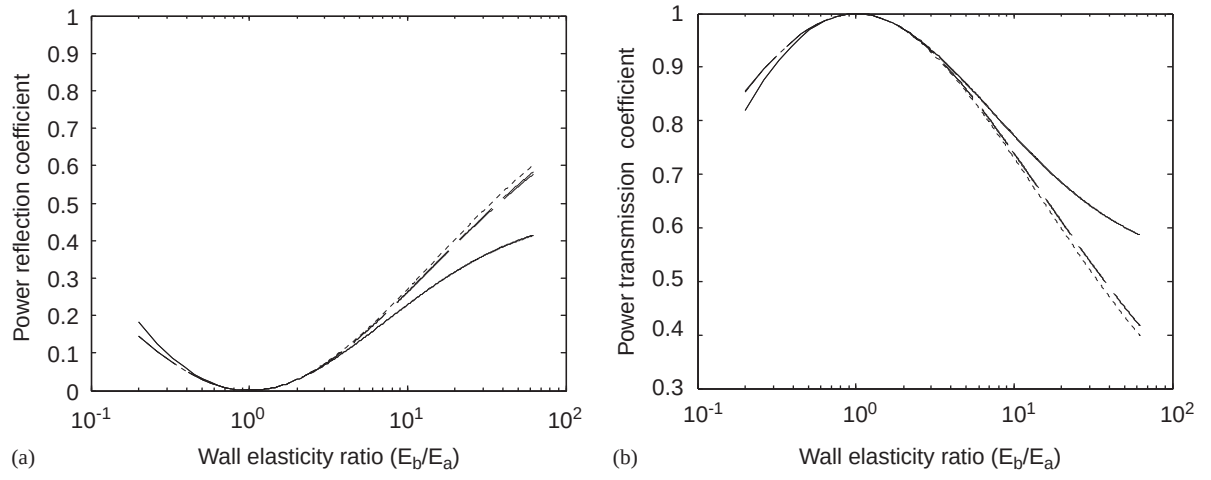

Fig. 5. (a) Power reflection coefficients. ——, $s_1 \to s_1$ and uncoupled approximation (not distinguishable); – – –, $s_2 \to s_2$ and uncoupled approximation (barely distinguishable; the uncoupled approximation is the upper curve); - - - - -, unloaded approximation. (b) Power transmission coefficients. ——, $s_1 \to s_1$ and uncoupled approximation; – – –, $s_2 \to s_2$ and uncoupled approximation; - - - - -, unloaded approximation.

4.3. Variation with pipe wall radius

Figs. 6a and b show the power reflection and transmissions coefficients for the MDPE pipe described in Table 1a coupled to a similar pipe with a different radius. The results are shown as a function of radius ratio, for $k_f a_a = 0.2$.

For comparison the reflection and transmission coefficients for the $s=1$ wave for a rigid walled pipe system is shown, along with the reflection and transmission coefficients for the $s=2$ wave for a non-fluid-loaded (i.e. empty) pipe system. For a rigid-walled system, the $s=1$ power reflection and transmission coefficients are given by

$$R_{aa11} = \left(\frac{1-(a_b/a_a)^2}{1+(a_b/a_a)^2}\right)^2 \quad \text{and} \quad T_{ab11} = \frac{4(a_b/a_a)^2}{(1+(a_b/a_a)^2)}. \tag{33a,b}$$

For an empty pipe system, the $s=2$ power reflection and transmission coefficients are given by

$$R_{aa22} = \left(\frac{1-a_b/a_a}{1+a_b/a_a}\right)^2 \quad \text{and} \quad T_{ab22} = \frac{4a_b/a_a}{(1+a_b/a_a)^2}. \tag{34a,b}$$

What is immediately apparent from the figures is that the cross-terms are no longer negligible; for changes in cross-section there is significant mode conversion between the $s=1$ and $s=2$ wavetypes. The mechanism for this is evident: for changes in elastic modulus or wall thickness, the boundary conditions at the junction are essentially uncoupled in that each condition relates *either* shell quantities *or* fluid quantities. For changes in pipe cross-section, two of the boundary conditions (continuity of total axial force and relative fluid volume velocity) relate shell *and* fluid quantities; physically, the pressure in the fluid acts directly on the shell at the change in cross-section and the forces in the shell act directly on the fluid.

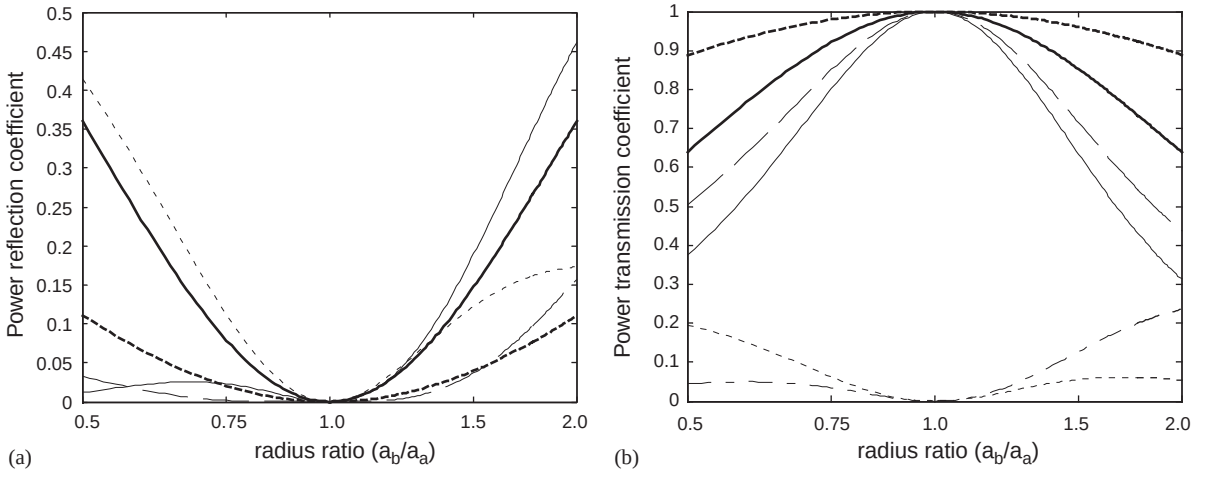

Fig. 6. (a) Power reflection coefficients. ——, $s_1 \to s_1$; – – –, $s_2 \to s_2$; - - - -, $s_1 \to s_2$; - - - - -, $s_2 \to s_1$; ——, rigid-walled approximation; – – –, unloaded approximation. (b) Power transmission coefficients. ——, $s_1 \to s_1$; – – –, $s_2 \to s_2$; - - - -, $s_1 \to s_2$; - - - - -, $s_2 \to s_1$; ——, rigid-walled approximation; – – –, unloaded approximation.

From Fig. 6a it can be seen that, for reductions in cross-section, the $s=1$ wave is predominantly reflected as an $s=2$ wave, and the $s=2$ wave is predominantly reflected as an $s=1$ wave, the proportion of energy reflected in each case being approximately equal to the $s=1$ energy that would be reflected in the rigid-walled case. The energy reflected and retained as its original wavetype is small. The overall amount of energy reflected for the incident $s=1$ wave is slightly greater than for the rigid-walled case. The overall amount of energy reflected for the incident $s=2$ wave is substantially greater than for the unloaded pipe case. For increases in cross-section, the $s=1$ wave is predominantly reflected as an $s=1$ wave, the proportion of energy reflected being approximately equal to the $s=1$ energy that would be reflected in the rigid-walled case. Significant $s=1$ energy is also reflected as $s=2$ energy, with the total energy reflected for an incident $s=1$ wave being much greater than for the equivalent rigid-walled case. For the $s=2$ incident wave, the energy reflected as an $s=2$ wave is approximately the same as if the pipes were unloaded (i.e. empty); however, some additional energy is reflected as an $s=1$ wave.

Examination of Fig. 6b reveals that, for both increases and decreases in cross-section, the $s=1$ wave is predominantly transmitted as an $s=1$ wave, and the $s=2$ wave is predominantly transmitted as an $s=2$ wave; the proportion of energy transmitted is less than for the equivalent rigid-walled and unloaded cases, respectively. A small amount of mode conversion for both wavetypes also occurs; for decreases in cross-section proportionally more energy is converted from the $s=1$ mode to the $s=2$ mode than vice versa; for increases in cross-section, the reverse is the case. The total amount of transmitted energy is less than for the equivalent rigid-walled and unloaded cases, as correspondingly more energy is reflected.

5. Effects of a surrounding medium

To describe the effects of a surrounding medium on the wave behaviour at the discontinuity completely, a fully coupled analysis of the discontinuity (including the pipe structure, contained fluid and surrounding medium) would need to be undertaken. However, it has been shown previously [4–6] that the effects of the surrounding medium are small compared with the effects of the shell walls (in the case of the $s=1$ wave) or contained fluid (in the case of the $s=2$ wave). Given this, a more simple approach has been taken which allows the more important features to be evaluated.

The presence of a fluid or solid medium around the pipe will have an impact in a number of ways. Firstly, the $s=1$ and $s=2$ wavenumbers will change; the surrounding medium will tend to mass load the pipe (affecting the wavespeeds in each section of pipe), and the waves may radiate, affecting the wave attenuation. How the wavenumbers are affected has been studied in detail previously [4–6], and is summarised in Section 2 of this paper.

The relationship between the wave pressures, shell axial and radial velocities, and shell axial forces will also be modified, as radiation impedance terms need to be included.

It is found that the radial shell velocities for the $s=1$ and $s=2$ waves, W_1 and W_2 respectively, are given by

$$W_1 = P_1 \frac{1}{(z_{\text{pipe}} + z_{\text{rad1}})} \quad \text{and} \quad W_2 = -P_2 \frac{1}{z_{\text{fluid}}}. \tag{35a,b}$$

The axial shell velocities, U_1 and U_2, are found to be

$$U_1 = P_1 \frac{-\mathrm{i}\nu}{k_1 a} \frac{1}{(z_{\text{pipe}} + z_{\text{rad1}})} \quad \text{and} \quad U_2 = P_2 \frac{\mathrm{i}}{\nu k_2 a} \frac{1}{z_{\text{fluid}}} \left(1 + \frac{(1-\nu^2)(z_{M\text{pipe}} + z_{\text{fluid}} + z_{\text{rad2}})}{z_{K\text{pipe}}}\right). \tag{36a,b}$$

The shell axial forces are given by

$$F_1 = P_1 \frac{2\pi\nu}{k_f^2} \frac{z_{M\text{pipe}}}{(z_{\text{fluid}} + z_{\text{pipe}} + z_{\text{rad1}})} \quad \text{and} \quad F_2 = P_2 \frac{2\pi a^2}{\nu} \left(1 + \frac{z_{\text{pipe}} + z_{\text{rad2}}}{z_{\text{fluid}}}\right). \tag{37a,b}$$

Finally, the wavenumber discontinuity in the pipe wall and contained fluid at the pipe discontinuity will mean that there must also be a wavenumber discontinuity in the surrounding medium. This will cause wave reflections in the surrounding medium, which will in turn affect the radiation loading on the pipe; in addition, when there is a change in pipe cross-section, the loading on the pipe due to the surrounding medium will act in the axial direction as well as radially, at the discontinuity. The reflections in the surrounding medium are accounted for in the analyses simply through the radiation impedance term associated with each positive- or negative-going wave. This approach does not necessarily ensure continuity and equilibrium axially in the surrounding medium at the pipe discontinuity, but is considered to constitute a good first-order approximation. For changes in cross-section, the axial loading of the pipe by the surrounding medium has also been neglected, but is judged to be small compared with the internal loading.

Simulations have been carried out with both water as the surrounding medium, which can support a compressional wave, and with unsaturated sand, which can support both shear and compression. For changes in wall thickness, as for the in vacuo case, negligible mode conversion occurs; the s_1–s_1 reflection and transmission coefficients can be approximated by Eqs. (30a) and (30b) with the modified wavenumbers calculated from Eq. (5) indicating that the change in wavenumber at the pipe junction dominates the behaviour as for the in vacuo case; likewise, the s_2–s_2 reflection and transmission coefficients can be approximated by Eqs. (31a) and (31b), the behaviour being controlled simply by the wall thickness change. For changes in wall elasticity also, the reflection and transmission coefficients can be approximated in the same way as for the in vacuo case (Eqs. (30a,b) and (32a,b)) with the wavenumbers in Eq. (30) being appropriately modified using Eq. (5). For changes in cross-section, the observed trends are similar to those discussed in Section 4.3 for the in vacuo case and shown in Figs. 6a and b.

6. Summary

In this paper, the wave transmission and reflection characteristics of the axisymmetric $s=1$ (fluid-dominated) and $s=2$ (shell dominated) waves at an axisymmetric pipe wall discontinuity in a fluid-filled piping system have been investigated. Soft-walled pipes were considered and the coupled nature of the two wavetypes was taken into account. The effects of a surrounding medium were also examined. The discontinuities considered were: a change in wall thickness, a change in pipe wall material elastic modulus, and a change of internal fluid cross-section.

It was found that, for a change in wall thickness or a change in wall elasticity, provided the fluid cross-section does not change, negligible mode conversion occurs at the discontinuity. Furthermore, the power reflection and transmission coefficients can be determined by considering each wavetype separately. For the $s=1$, fluid-dominated, wave, the reflection and transmission coefficients can be found by considering only the wavenumber change at the discontinuity. For the $s=2$, shell dominated, wave, the coefficients can be found by assuming that the pipe is empty and considering the thickness change or elasticity change only, as appropriate. For the case of a change in wall elasticity, a slightly improved approximation can be made by considering the total wavenumber change at the discontinuity. The above findings are still valid when the pipes are buried or immersed, provided that the effects of the surrounding medium are accounted for in determining the wavenumbers.

When there is a change in fluid cross-section it was found that mode conversion occurs between the two wavetypes. In this case, the waves can no longer be treated separately, and must be considered together. In general, more energy is reflected (and correspondingly less transmitted) than for the equivalent rigid-walled or unloaded case. For reductions in cross-section, for each of the two wavetypes most of the energy is converted to the other wavetype on reflection. For increases in cross-section, most of the energy is not converted between wavetypes. For both increases and decreases in cross-section, the transmitted energy is predominantly retained as its original wavetype.

Successful leak detection using correlation techniques relies on a significant amount of acoustic energy being transmitted along the pipelines away from the leak. In the modelling, it has been assumed that the sections of pipe are of semi-infinite extent either side of the discontinuity. In practice, however, a replacement section of pipe will be of finite length, so resonant behaviour will be observed, depending on the length of the replacement pipe, modifying the overall reflection and transmission coefficients. Notwithstanding this, the results reported here provide some useful insights into one of the mechanisms affecting the transmission of the leak noise energy. This will then better inform the water industry on both why leaks sometimes fail to be detected and also on ways leak detection capability might be improved in the future.

Acknowledgement

The EPSRC are gratefully acknowledged for their support of this work.

References

[1] H.V. Fuchs, R. Riehle, Ten years of experience with leak detection by acoustic signal analysis, *Applied Acoustics* 33 (1991) 1–19.

[2] O. Hunaidi, W.T. Chu, Acoustical characteristics of leak signals in water distribution pipes, *Applied Acoustics* 58 (1999) 235–254.

[3] O. Hunaidi, W.T. Chu, A. Wang, W. Guan, Detecting leaks in plastic water distribution pipes, *Journal of the American Water Works Association* 92 (2000) 82–94.

[4] J.M. Muggleton, M.J. Brennan, R.J. Pinnington, Wavenumber prediction of waves in buried pipes for water leak detection, *Journal of Sound and Vibration* 249 (2002) 939–954.

[5] J.M. Muggleton, M.J. Brennan, P.W. Linford, Axisymmetric wave propagation in fluid-filled pipes: wavenumber measurements in *in vacuo* and buried pipes, *Journal of Sound and Vibration* 270 (2004) 171–190.
[6] J.M. Muggleton, M.J. Brennan, Leak noise propagation and attenuation in submerged plastic water pipes, *Journal of Sound and Vibration* 278 (2004) 527–537.
[7] R.J. Pinnington, A.R. Briscoe, Externally applied sensor for axisymmetric waves in a fluid filled pipe, *Journal of Sound and Vibration* 173 (1994) 503–516.
[8] C.R. Fuller, F.J. Fahy, Characteristics of wave propagation and energy distributions in cylindrical elastic shells filled with fluid, *Journal of Sound and Vibration* 81 (1982) 501–518.
[9] C.R. Fuller, The effects of wall discontinuities on the propagation of flexural waves in cylindrical shells, *Journal of Sound and Vibration* 75 (1981) 207–228.
[10] E.H. Kennard, The new approach to shell theory: circular cylinders, *Journal of Applied Mechanics* 20 (1953) 33–40.
[11] D.I. Korteweg, Über die Fortpflanzungsgeschwindigkeit des Schalles in elastischen Röhren (On the speed of sound in water in flexible pipes), *Ann Physik* 5 (1878).